Performance Analysis of Power Line Communication System for Massive Indoor IoT Applications

Mai Hassan[1], Hesham G. Moussa[1], and Pin-Han Ho[1]
[1] Department of Electrical and Computer Engineering,
University of Waterloo, Waterloo, ON, Canada

This study explores the utilization of low-voltage indoor power line communication (PLC) technology within the framework of a split centralized radio access network (C-RAN) architecture, aimed at enhancing 5G indoor mobile coverage for the Internet of Things (IoT). A primary focus of this investigation is the comprehensive evaluation of the system's performance in terms of radio and access latency. Several critical variables come into play, including available bandwidth, the chosen transmission technology, and the number of wireless IoT devices within the network. An analytical model, employing queuing theory, Markovian models, and stochastic geometry, is formulated to assess the radio-access delay spanning the air interface and the innovative PLC-based front-hauling system proposed in our previous study. The precision of this model is validated through simulations, ensuring that the proposed system effectively meets the stringent latency constraints required by eCPRI, thus contributing to the improvement of 5G indoor mobile coverage for the IoT network.

***Index Terms*—Massive Machine type communication (mMTC), Internet of things (IoT), Stochastic geometry, Queuing theory, Markovian models, Power Line communication (PLC).**

I. Introduction

In the split C-RAN architecture proposed as part of 5G New Radio (NR), radio units (RUs) are deployed within indoor sites, and are connected to the distributed unit (DU) through high-speed links known as front-haul [1]. This architecture is expected to enable various IoT-based indoor services. However, for this proposed architecture to prevail, extensive structural modifications are needed to extend the proper front-haul links throughout intended indoor sites. This creates a trade-off between the cost of deployment and convenience. As such, a potentially cost-effective way of establishing front-haul links in buildings is to capitalize the inherent network of power lines stretched across the fabric of the construction to enable connectivity via power-line communication (PLC) technology [2], [3].

While impulsive noise and other particular issues make PLC less desirable as a communication medium, in our earlier study [4], we argued that PLCs can be used to support enhanced Common Public Radio Interface (eCPRI)-based front-hauling for 5G indoor mobile coverage. To fulfill the strict bit error rate criteria for eCPRI, we suggested a system and a technique. Continuing from that, and to further support our argument of the possibility of using PLC front hauling to enable massive indoor IoT applications, the contributions of this study is a mathematical end-to-end delay performance model throughout the radio access network (RAN) that takes into account the newly suggested PLC-based front-haul system from [4] as well as wireless radio interface delay. The created model defines the delay as a function of the number of deployed RUs, wireless IoT devices, and the underlying bandwidth and transmission technology of the PLC-based front-haul. Principles from both queuing theory and stochastic geometry are used to capture complex relations between various parameters. Using the developed model, we show that, in the proposed system, the over-the-air delay requirements can be achieved. We also show that for the low and medium class of services, the PLC one-way delay constraint can be inherently met, whereas, for high class of services, further research is needed to satisfy the requirements. The accuracy of the developed end-to-end model is proven via extensive simulations.

The paper is organized as follows. Section II presents the system model. Detailed end-to-end performance analysis is provided in Sections III and IV. Section V provides the simulation results, and Section VI concludes the paper. Table I provides a summary of the symbols used to define the problem and derive the mathematical expressions.

Manuscript received: October 22, 2023; revised: December 13,2023.
Corresponding author: Mai Hassan (email: mai.hassan@uwaterloo.ca).

II. Background and Literature Review

A. 5G Split Centralized Radio Access Network

In the split C-RAN architecture, the radio frequency and base-band processing functionalities are separated across three logical nodes: a central unit (CU), DU, and RU, each with its own 5G NR stack function. This innovative design enables the deployment of RUs within buildings to achieve highly effective CU at the central station through high-speed links known as front-haul links. Figure 1 shows a descriptive schematic of the split C-RAN architecture [1]. Nevertheless, when implementing massive machine type communication (mMTC) applications in indoor environments with split C-RAN, a crucial balance must be struck between the cost of necessary infrastructural modifications and the achievable quality of service levels. This trade-off becomes particularly significant when dealing with applications that demand stringent delay constraints [5].

TABLE I: Summary of important mathematical symbols

Symbol	Description
$\mathcal{V}_a$	The area of the Voronoi cell of a RU
T_a	Duration of 1 frame over 5G air interface
M_{tot}	Total No. of identical IoT devices within network
M_j^t	No. of devices in the cluster associated to j^{th}RU
M_{max}	Max number of devices a RU schedules in a single TR
$M_{a_j}^t$	No. of active devices associated with j^{th} RU in t^{th} TR
$M_{c_j}^t$	No. of covered scheduled devices associated with j^{th} RU in t^{th} TR
$\mathcal{M}_a^t$	Mean number of active devices connected to RU
Q_i^r	Power received at the RU located at the origin from associated device located at $d_i^{n,t}$ after FPC
P_a	The nominal transmission power of any device
ϵ_a	The power control factor $\in \{0,1\}$
α_a	The path-loss exponent over the air interface
g_{ij}	Rayleigh fading radio ch. bet. i^{th} device & j^{th} RU
σ_a^2	Radio AWGN received noise power
Φ	Set containing the locations of the RUs ($_b$) or all IoT devices ($_d$) or active devices ($_a$)
$b_j,\ d_i$	2-D location of the j^{th} RU & i^{th} device in network
λ	The RU ($_b$), total device ($_d$) or active devices ($_a$) density per unit area
Ω	Total bandwidth of radio ch. ($_a$) or PLC ch. ($_p$)
$\mathcal{N}$	Total number of sub-channels over air interface ($_a$) or PLC front-haul ($_{plc}$)
γ_d	Poisson process parameter of data generated at device
$\mathcal{D}$	The number of bits in the radio data-frame ($_a$) or the PLC eCPRI-frame ($_p$)
$\mathcal{P}_s$	Conditional scheduling probability in the current TR
$\Theta_0^{n,t}$	Received SINR level at RU_0 of data-frame transmitted by $device_0$ on n^{th} sub-channel and during t^{th} TR
τ_a	The SINR threshold defining RU's coverage area
I_a	Inter-cell interference experienced by a device
$C_0^{n,t}$	Device-RU coverage probability for the device located at $d_0^{n,t}$ and served by the RU at the origin
$\mathcal{C}_a$	Unconditional coverage probability over radio channel
$\mu_a^{n,t}$	Device's service rate for n^{th} sub-channel during t^{th} TR
$\mathcal{R}_a^n$	Average bit rate of i^{th} device which is in coverage, and scheduled on n^{th} sub-channel
$\mathcal{R}_p^j$	eCPRI data rate from j^{th} RU into eCPG
$\mathcal{R}_p$	Total data rate at PLC link from FDMA sub-channels
Λ_{ap}	Conversion factor between data rate over air interface & required data rate for eCPRI-frame
T_q	Incoming queuing delay at the R-eCPG until the new eCPRI-frame is transmitted
T_{ts}	Transport delay through the PLC channel

The implementation of a split C-RAN design enhances resource utilization, reduces energy consumption, and mitigates interference through features like Coordinated Multi-point (CoMP) [6], [7]. Split C-RAN also facilitates eco-friendly and cost-effective communication [8]. Studies confirm significant savings in both operating cost (OPEX) and Capital cost (CAPEX) with a centralized architecture. Notably, China's adoption of the C-RAN layout resulted in a substantial 70% reduction in the OPEX of the base station infrastructure [9]. Despite these advantages, a primary challenge in 5G C-RAN involves establishing a reliable front-haul link between DU and RUs. This front-haul link is crucial for delivering high capacity, low latency, reliable, and efficient cost and energy usage [8].

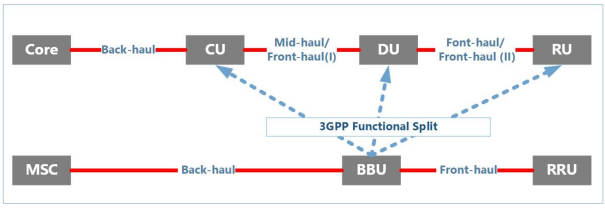

Fig. 1: The Split C-RAN architecture

In split C-RAN, the front-haul link is expected to handle both uplink (RU to DU) and downlink (DU to RU) radio signals while satisfying standardized performance KPIs. Yet, depending on the physical attributes of the Front-Haul link, a significant amount of additional latency could be introduced compared to traditional distributed layouts [10]. As such, optimizing the Front-Haul in split C-RAN is crucial as it must be designed such that it is able to deliver high bandwidth to meet the demands of multiple RUs. Various transport media have been considered to build front-haul links, including optical fiber, wireless links, and copper cables. Each media has advantages and disadvantages. For instance, while optical fiber is optimal due to its large bandwidth and low latency, it is also the most expensive choice. Alternatively, options like coaxial cable and CAT 5/6/7 cables have been explored, but each faces challenges in indoor settings, as their installation can be impractical and costly. They also lack ubiquity and are not inherently present in the structures of the buildings. Notably, all these options may necessitate external power sources for indoor RUs which present an additional layer of complexity and cost.

B. Power-Line Communication

In contrast, buildings have inherent networks of power lines already embedded into their fabric. Those power lines, in addition to being used to carry power, and according to recent research, can also be adapted as communication links to carry data under the paradigm of PLC. The ubiquity of power lines and the fact that they are naturally embedded into the construction of the building makes PLC a potentially economical and reliable technology that may enable diverse applications, including smart homes, smart

grids, and broadband connections [11], [12]. PLC technology advantages lie in utilizing existing indoor power lines without the need for infrastructure modifications. furthermore, the power line medium, analogous to radio frequency bands, operates in an unrestricted, unlicensed manner, eliminating additional costs for consumers and the dependence on external power sources. PLC, requiring no licensing, is particularly suitable for establishing point-to-point connections [13].

Despite PLC's prevalence in indoor broadband services, it faces distinct challenges. The PLC channel, characterized by log-normal frequency-dependent attenuation, introduces complexities in signal transmission [14], [15]. Susceptibility to the background and impulsive noises, particularly the spontaneous nature of the latter, poses a formidable obstacle to data integrity across power lines, challenging conventional coding methods [16]. Consequently, according to the authors' knowledge, Our previous research [4], [17] is a novel solution regarding the usage of low voltage power-lines as transmission media for the front-haul link. In addressing these challenges for 5G NR front-hauls in [4], we introduced a novel solution: the evolved eCPRI-PLC Gateways (eCPGs). In addressing these challenges for 5G NR front-hauls, the authors in [4] have introduced a novel solution: the evolved eCPRI-PLC Gateways (eCPGs). Acting as intermediaries, the eCPG creates virtual eCPRI links between the RU and DU, enabling desired eCPRI options despite the noisy PLC channel. The authors have shown that the eCPG is an effective module that enables the use of power-line communication as a transmission media for the C-RAN front-haul.

III. System Model

A. Radio-Access Architecture

In a multi-story indoor service building environment, a large number of wireless IoT devices are distributed randomly. These IoT devices serve the purpose of collecting data that is sensitive to errors and delays. This data needs to be transmitted to multiple service owners. In the proposed system, The network employs a split C-RAN system, as depicted in Figure 2, the Front-Haul link consists of two segments: a Mid-haul/front-haul (I) segment connecting the CU and DU through optical fiber and a front-haul (II) segment linking the DU to various indoor RUs. It's worth noting that this research does not cover the specifics of the technology used in front-haul (I).

In Figure 3 the indoor radio access network architecture is illustrated where several RUs are scattered randomly throughout the building to facilitate the operation of the IoT devices. Each RU is connected to a power socket, providing both power and access to the PLC front-haul. Each RU and DU is linked to eCPG, designated as R-eCPG and D-eCPG, respectively [4]. The eCPG serves as a plug-and-play device facilitating the connection between the front-haul system and power lines without necessitating modifications to the DU and RU. The D-eCPG is connected to the indoor Power Distribution Unit (PDU) through a 5-conductor three-phase line. Beyond the PDU, each power socket is supplied with one of the single-phase lines containing three types of conductors: Phase/Live (P), Neutral (N), and Protective Earthing (PE).

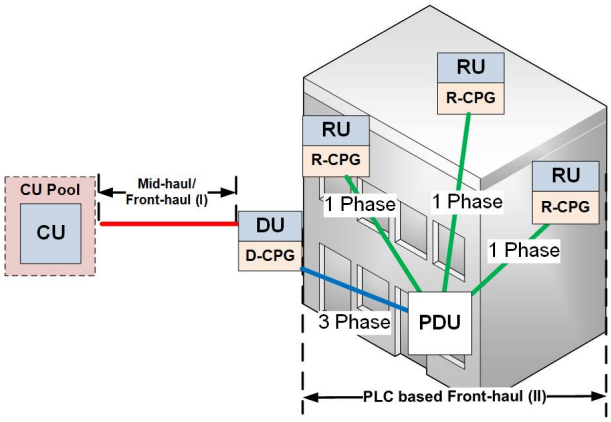

Fig. 2: Indoor/outdoor C-RAN system

The front-haul (II) segment is responsible for transmitting eCPRI messages using standard Ethernet frames to and from the indoor RUs. For the remainder of this paper, eCPRI messages sent in IP/Ethernet frames or UDP/IP datagrams are simply referred to as eCPRI-frames, unless stated otherwise. In order to make effective use of the PLC-based front-haul for the final connection, several transmission techniques are implemented to address the challenging conditions of the PLC channel. These techniques encompass mechanisms like Impulsive noise detection & re-transmission (IND) and Selective repeat-based Hybrid Automatic Repeat request (HARQ), which have been previously introduced in out prior research studies [4], [17]. To facilitate this process, a pair of devices, denoted as evolved eCPRI-PLC Gateways (eCPGs), is strategically deployed at both the RU and DU locations. Specifically, the eCPG associated with the RU is known as R-eCPG, while the one connected to the DU is referred to as D-eCPG.

The PLC link utilizes eCPRI option 7-2, specifically Splits II_D and II_U, which represent IQ-oriented splits for the downlink and uplink [18]. These splits are the most demanding in terms of front-haul throughput and latency. As for the wireless air interface, a 5G orthogonal frequency-division multiplexing (OFDM) radio channel is employed, with the service band shared among all the IoT devices. Consequently, devices associated with different RUs and scheduled on the same sub-channel may experience interference between cells.

B. Wireless Spatial Model

In the forthcoming analysis, we concentrate on assessing the system's performance for a single floor of the building independently, without accounting for interference between floors. To illustrate this, we consider a layer of cellular RUs connected to a DU, which is further

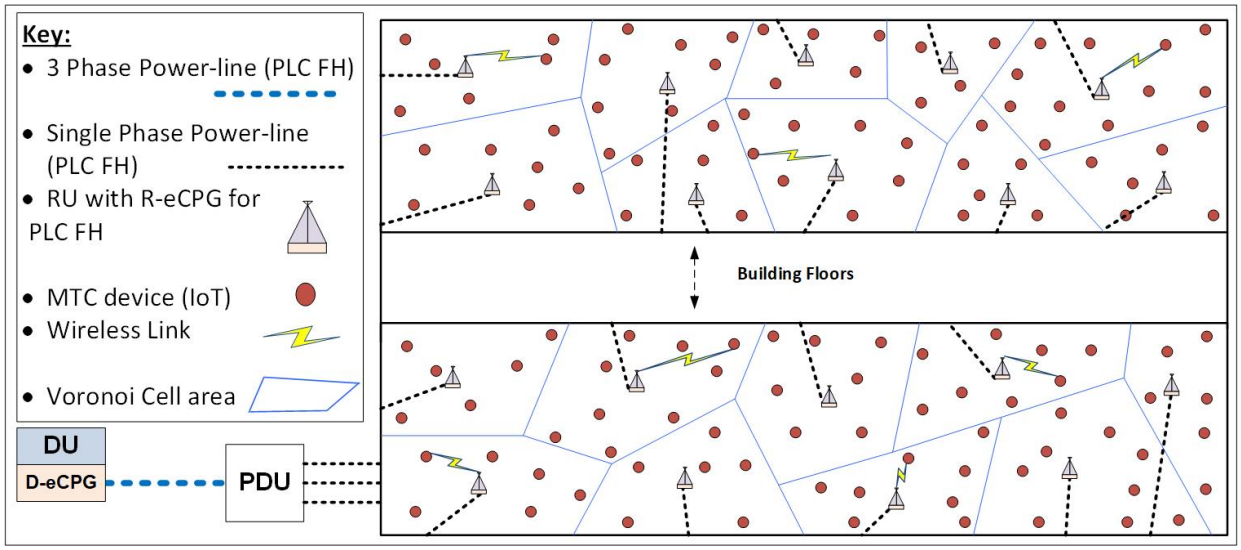

Fig. 3: Indoor Radio access network architecture

connected to the CU of the Base Station. The positions of these RUs within the building can be represented as a Homogeneous Poisson Point Process (HPPP), denoted as $\Phi_b = \{b_0, b_1, b_2, \ldots\}$. The density of RUs per unit area is referred to as λ_b, and b_j corresponds to the 2-D location of the j^{th} RU.

The network serves a large number of identical IoT devices, denoted as M_{tot}, which are randomly distributed across the specific floor of the building under consideration. The positions of these devices are modeled as an independent HPPP, denoted as $\Phi_d = \{d_0, d_1, d_2, \ldots\}$, with a device density per unit area of λ_d. Here, d_i represents the 2-D location of the i^{th} device in the network. The IoT devices can be in either an active or inactive state, depending on data availability for transmission.

Each active IoT device generates data-frames according to a Poisson process with a parameter $\gamma_d \in (0, \infty)$. The size of each data-frame transmitted over the air interface is $\mathscr{D}_a$ bits. Since our primary focus is on active devices, accurately modeling their locations is crucial. Using the concept of "Independent Thinning" from stochastic geometry, we can depict the locations of active devices as a thinned independent HPPP derived from the original HPPP that represents all devices in the network. We denote the set of active device locations as $\Phi_a \subseteq \Phi_d$, and it follows an independent HPPP with a density of $\lambda_a = \mathscr{A}^t \times \lambda_d$, where $\mathscr{A}^t$ denotes the probability that at least one data-frame is generated during the t^{th} Transmission Round (TR).

Once a device becomes active, it tries to associate with a RU based on the maximum received signal strength (max-RSS) association rule. Devices associate with RUs to form clusters. Each RU is responsible for relaying the data-frames generated by the devices in its cluster to the DU over the PLC-based front-Haul, which are subsequently transmitted to the core network. However, as each IoT device generates small-sized data-frames, adopting a per-data-frame relay framework would be inefficient in terms of front-haul resources. Thus, in this work, we assume that each RU can aggregate the small-sized data-frames generated by its associated IoT devices and convert them into the appropriate eCPRI transmission format before transmitting them over the PLC front-haul.

C. Wireless transmission Model

At the RUs, OFDMA is employed over the air interface channel. A shared uplink channel (SUCH) with a total bandwidth of Ω_a is split into orthogonal sub-channels with $\mathscr{N}_a$ equal bandwidth. Time is broken down into TRs, which consist of the following: the time needed for one 5G sub-frame $T_a = 1ms$; and the time needed to send the eCPRI-frame over the PLC front-haul T_{PLC}, which is defined later. Figure 4 depicts the transmission round structure. At the beginning of each TR, all active devices associated with an RU are assumed to have one data-frame to transmit. Let the random variable, M_j^t, denote the number of devices in the j^{th} cluster at the t^{th} TR, where $\sum_j M_j^t \leq M_{tot}$. M_j^t is a function of the association conditions, locations of devices and RUs, their densities, and the transmission power. RUs schedule at most one associated device per sub-channel such that a maximum M_{max} of devices are scheduled in a single TR where $M_{max} = \min\{M_{a_j}^t, \mathscr{N}_a\}$. $M_{a_j}^t$ denotes the number of active devices in the j^{th} cluster at the t^{th} TR and $M_{a_j}^t \leq M_j^t$.

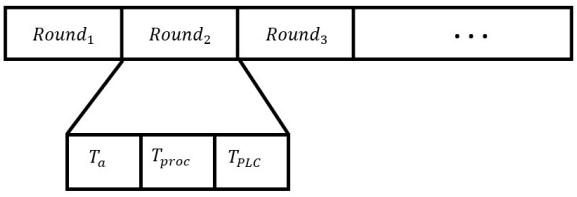

Fig. 4: Transmission Round (TR) structure

Inter-cell interference among devices in different clusters and scheduled on the same sub-channel results in transmission failure. Devices with successful transmission are said to be in coverage. A data-frame that fails to be transmitted in the current TR stays in the queue of the blocked device until the next TR. As such, define $M_{c_j}^t$ as the number of scheduled and covered devices, associated with the j^{th} RU during the t^{th} TR, such that $M_{c_j}^t \leq M_{max}$.

As in [19], the power received at the RU from an associated device is given as $Q_i^r = P_a ||d_i^{n,t} - b_j||^{(\epsilon_a - 1)\alpha_a} g_{i,j}$, where P_a is the nominal transmission power of any connected IoT device, $||d_i^{n,t} - b_j||$ is the Euclidean distance between the i^{th} device, scheduled on the n^{th} sub-channel, and its serving (j^{th}) RU during the t^{th} TR, $g_{i,j}$ is the power gain of the Rayleigh fading radio channel which follows an exponential distribution with unity mean (i.e., $g_{i,j} \sim \exp\{1\}$), and $\epsilon_a \in \{0,1\}$ is the power control factor. The radio channel also introduces additive white Gaussian noise with received noise power σ_a^2. Radio channel gains are uniformly distributed, independent of distance, and independent of one another (i.i.d.).

IV. Performance Modeling

A. Coverage Probability over wireless link

The probability that a data-frame sent from an IoT device will be successfully received by the serving RU is known as the coverage probability. It is a function of signal-to-interference-plus-noise ratio (SINR); a data-frame must be received with a SINR higher than a certain threshold (τ_a) in order for the RU to successfully decode it. Assuming that all active devices return to the device pool at the conclusion of a TR and that each RU has the same number of active devices at the start of each TR simplifies the analysis [19].

1) Scheduling Probability Calculations

In the following analysis, we focus on a typical device (device$_0$) located at d_0 and is being served by a typical RU (RU$_0$) that is located at the origin. It should be noted; however, that the analysis is also applicable for any device-RU pair [20].

Let the number of active devices associated with RU$_0$ in the t^{th} TR be denoted by the Random Variable (RV) $M_{a_0}^t$. The RV $M_{a_0}^t$ has a probability mass function (PMF) that is calculated by approximating the probability density function (PDF), over a Voronoi cell of area $\mathcal{V}_a$ as marked in Figure 3. As such, the PMF can be denoted by a generalized gamma distribution which is given by [19], [21]

$$\mathbb{P}(M_{a_0}^t = m) = \frac{(c_v.\lambda_b)^{c_v} \lambda_a^m \Gamma(m+c)}{\Gamma(c_v)(\lambda_a + c_v.\lambda_b)^{m+c_v}\ m!},\ 0 \leq m < \infty \quad (1)$$

where $c_v = (3d+1)/2 = 7/2$ is a constant defined for the Voronoi tessellation in $\mathbb{R}^2$ with dimensionality $d = 2$ and $\Gamma(c_v) = \int_0^\infty t^{c_v - 1} e^{-t} \mathrm{d}t$. Thus, the average number of active devices is calculated as [21]

$$\overline{M}_a^t = \mathbb{E}_m[M_a^t] = \left\lceil \frac{\lambda_a\ \Gamma(c_v+1)}{\lambda_b\ c_v.\Gamma(c_v)} \right\rceil \quad (2)$$

Let $\mathscr{P}_s$ be the conditional scheduling probability conditioned on the number of active devices in the t^{th} TR denoted by $M_{a_0}^t = m$. Averaging over the PMF given in (1), the scheduling probability of an active IoT device is given by [20]

$$\begin{aligned} \mathscr{P}_s &= \mathbb{E}_{M_{a_0}^t}\left[\frac{\min\{M_{a_0}^t, \mathscr{N}_a\}}{M_{a_0}^t} \middle| M_{a_0}^t = m \right] \\ &= \mathbb{E}_{M_{a_0}^t}\left[\frac{\mathscr{N}_a}{\max\{M_{a_0}^t, \mathscr{N}_a\}} \middle| M_{a_0}^t = m \right] \\ &= \sum_{m=0}^{\mathscr{N}_a} \frac{(c_v.\lambda_b)^{c_v} \lambda_a^m \Gamma(m+c)}{\Gamma(c_v)(\lambda_a + c_v.\lambda_b)^{m+c_v}\ m!} \\ &+ \sum_{m=\mathscr{N}_a+1}^{\infty} \frac{\mathscr{N}_a}{m} \frac{(c_v.\lambda_b)^{c_v} \lambda_a^m \Gamma(m+c)}{\Gamma(c_v)(\lambda_a + c_v.\lambda_b)^{m+c_v}\ m!} \end{aligned} \quad (3)$$

where $\frac{\min\{M_{a_0}^t, \mathscr{N}_a\}}{M_{a_0}^t}$ reflects ratio of the number of active devices that have been scheduled. The expression $\min\{M_{a_0}^t, \mathscr{N}_a\}$ ensures the probability of scheduling is limited by the minimum of the two values: number of radio sub-channels per RU and number of active devices within the RU Voroni cell.

2) SINR calculations

Let $\Theta_{0,0}^{n,t}$ denote the received SINR level of the data-frame transmitted by the device located at position d_0 on the n^{th} sub-channel, during the t^{th} TR, and received at RU located at b_0 denoted as RU$_0$ to be given by

$$\Theta_{0,0}^{n,t} = \frac{P_a ||d_0^{n,t} - b_0||^{(\epsilon_a - 1)\alpha_a} g_{0,0}}{I_a + \sigma_a^2}, \quad n \in \{1, 2, ..., \mathscr{N}_a\} \quad (4)$$

where σ_a^2 is the received additive Gaussian noise, and I_a is the inter-cell interference experienced by each device.

Devices experience inter-cell interference from other devices served by other RUs within the network and are scheduled on the same sub-channel. Accordingly, an independent thinned PPP ($\Phi_a^{n,t} = \{d_1^{n,t}, d_2^{n,t}, ...\}$) with density $\lambda_a^{n,t} = \lambda_b$ represents the locations of the inter-cell active device (i.e. in other clusters) interfering on the n^{th} sub-channel during the t^{th} TR. Thus, the interference can be modeled as

$$I_a = \sum_{d_i^{n,t} \in \Phi_a^{n,t}} P_a ||d_i^{n,t} - b_j||^{\epsilon_a \alpha_a} ||d_i^{n,t} - b_0||^{-\alpha_a} g_{i,0} \quad (5)$$

where $g_{i,0}$ is the radio channel gain between the i^{th} device and RU$_0$. $||d_i^{n,t} - b_0||$ denotes the Euclidean distance between the i^{th} inter-cell interfering device and the non-serving RU$_0$ located at the origin, and $||d_i^{n,t} - b_j||$ is the Euclidean distance between the i^{th} inter-cell interfering device and its serving RU (the j^{th} RU, where $j \neq 0$). Note that $||d_0^{n,t} - b_0||$, $||d_i^{n,t} - b_0||$ and $||d_i^{n,t} - b_j||$ are all random

distances as they depend on the locations of the considered device and RU pair. Considering that $g_{0,0}$ and $g_{i,0}$ are exponentially distributed with unity mean, the scheduled device-RU coverage probability for the device located at $d_0^{n,t}$ and served by RU_0 can be expressed as [20]

$$\begin{aligned} C_{0,0}^{n,t} &= \mathscr{P}_s.\mathbb{P}(\Theta_{0,0}^{n,t} > \tau_a) \\ &= \mathscr{P}_s.exp\left\{-\frac{\tau_a}{P_a} r_t^{\alpha_a(1-\epsilon_a)} \sigma_a^2\right\}.\mathscr{L}_{I_a}\left\{\frac{\tau_a}{P_a} r_t^{\alpha_a(1-\epsilon_a)}\right\} \end{aligned} \quad (6)$$

where $r_t = ||d_0^{n,t} - b_0||$ is used to denote the distance between the device of interest and the origin during the t^{th} TR, $\mathscr{L}_{I_a}\{z\}$ is the Laplace transform of z with respect to inter-cell interference I_a, and $\mathscr{P}_s$ is defined in (3).

3) Inter-cell Interference calculations

Let $s = (\tau_a/P_a).r_t^{\alpha_a(1-\epsilon_a)}$, then the conditional coverage probability conditioned on the distance r_t to the nearest RU can be written as

$$C_{0,0}^{n,t}(\sigma_a, \tau_a, \lambda_d^{n,t}, \alpha_a, \epsilon_a | r_t) = \mathscr{P}_s.\exp\{-s\sigma_a^2\}\mathscr{L}_{I_a}\{s\} \quad (7)$$

where, using Campbell's theorem, $\mathscr{L}_{I_a}\{s\}$ can be expressed as [19]

$$\begin{aligned} \mathscr{L}_{I_a}\{s\} = \mathscr{L}_{I_a}\left\{\frac{\tau_a}{P_a} r_t^{\alpha_a(1-\epsilon_a)}\right\} \approx \exp\Big(-2\pi\lambda_d^{n,t}\int_{x_t>0}\Big[1 \\ -\int_{y_t>0}\frac{2\pi\lambda_a y_t e^{(-\pi\lambda_a y_t^2)}}{1+\tau_a r_t^{(1-\epsilon_a)\alpha_a} y_t^{\epsilon_a\alpha_a} x_t^{-\alpha_a}}\mathrm{d}y_t\Big]x_t\,\mathrm{d}x_t\Big) \end{aligned} \quad (8)$$

such that $y_t = ||d_i^{n,t} - b_j||$ denotes the distance between a device located at $d_i^{n,t}$ and its serving RU located at b_j, and $x_t = ||d_i^{n,t} - b_0||$ denotes the distance between the i^{th} device located at $d_i^{n,t}$ and using the n^{th} sub-channel and RU_0 during the t^{th} TR. r_t, y_t, and x_t all follow Rayleigh distributions with parameters λ_b, λ_a and $\lambda_d^{n,t}$ respectively.

Since the preceding analysis is applicable to any device-RU pair, let the general radio coverage probability for any scheduled device-RU pair be denoted by $\mathscr{C}_a$. For simplicity, let R_t be the random distance between a device and its serving RU. The average unconditional coverage probability, $\mathscr{C}_a = \mathscr{P}_s.\mathbb{E}_{R_t}[C_0^{n,t}(\sigma_a, \tau_a, \lambda_b, \alpha_a, \epsilon_a | R_t)]$, at any TR, is approximated as [20]

$$\begin{aligned} \mathscr{C}_a \approx 2\pi\lambda_b.\mathscr{P}_s.\int_{r_t>0}\exp\Big(-\pi\lambda_b r_t^2 - \frac{\tau_a}{P_a} r_t^{(1-\epsilon_a)\alpha_a}\sigma_a^2 - 2\pi\lambda_b. \\ \int_{x_t>0}\left[1-\int_{y_t>0}\frac{2\pi\lambda_a y_t e^{(-\pi\lambda_a y_t^2)}}{1+\tau_a r_t^{(1-\epsilon_a)\alpha_a} y_t^{\epsilon_a\alpha_a} x_t^{-\alpha_a}}\mathrm{d}y_t\right]x_t\,\mathrm{d}x_t\Big).r_t\mathrm{d}r_t \end{aligned} \quad (9)$$

where the PDF for the distance between a scheduled device and its serving RU is set as $f_R(r_t) = 2\pi\lambda_a r_t e^{-\pi\lambda_a y_t^2}$. The mean number of covered IoT devices is calculated as

$$\overline{M_c^t} = \left\lceil \mathscr{C}_a.\overline{M_a^t} \right\rceil \quad (10)$$

B. Delay over the air interface

The overall delay of a data-frame consists of two elements: first link delay (the queuing time at the source device before successful transmission (Device-RU)), and second link delay (the time the eCPRI-frame spends in transmission queues at the R-eCPG to the D-eCPG over the PLC-based front-haul network) [4]. As such, this can be thought of as a tandem queue model where the incoming rate into the second queue depends on the output rate of the first queue. With this in mind, in this section, we analyze the first queue that occurs at the IoT device buffer.

For the first link delay, a device is able to transmit its data-frame successfully if it is associated with an RU, is scheduled on an OFDM-based sub-channel, and is in coverage. Let the queuing delay at a device, defined as the mean number of 5G frames' time (T_a) needed for the device to successfully connect to its serving RU and successfully transmit a single data-frame, be denoted by $\overline{\Gamma_a}$. The device-RU coverage probability given in equation (9) determines the geometric distribution used to represent $\overline{\Gamma_a}$, as in [20]. As such, the mean over-the-air delay is given as $\overline{\Gamma_a} = (T_a/\mathscr{C}_a)$ [20]. Alternatively, let the device's service rate for the n^{th} sub-channel and during the t^{th} TR be defined as [20]

$$\mu_a^{n,t} = \left\lfloor \frac{T_a \mathscr{R}_a^n}{\mathscr{D}_a} \right\rfloor \quad n = 1, 2, \ldots, \mathscr{N}_a \quad (11)$$

where $\mathscr{R}_a^n$ defines the mean bit rate achievable by the i^{th} device which is in coverage, located at $d_i^{n,t}$, and scheduled on the n^{th} sub-channel of the RU located at the origin. Note that $\mathscr{R}_a^n$ is conditioned on the probability that the device is scheduled on a sub-channel and is in coverage (i.e $\Theta_0^{n,t} > \tau_a$). Additionally, in (11), the flooring function is to ensure that only fully successfully transmitted data-frames are taken into account. It should be clear that $\mathscr{R}_a^n$ defines the average departure/service rate of data-frames at a typical device which, as will be discussed, can be used to calculate the delay performance of the first link.

Using Shannon's formula, we have $\mathscr{R}_a^n = \mathbb{E}[\omega_a \log_2(1+\Theta_0^{n,t}) \mid \Theta_0^{n,t} > \tau_a \;\&\; \mathscr{X} = 1]$, where $\mathscr{X} = [0,1]$ defines the scheduling status such that $\mathscr{X} = 0$ indicates the device is not scheduled and $\mathscr{X} = 1$ indicates otherwise. With no closed-form PDF expression for the SINR, $\mathscr{R}_a^n$ is calculated as the maximum of two values, namely: a lower bound $\mathfrak{L}_a^n = \omega_a \log_2(1+\tau_a)$ (a fixed allocation of the bit rate), and the unconditional mean achievable bit rate, $\mathscr{F}_a^n = \mathbb{E}\left[\omega_a \log_2(1+\Theta_0^{n,t})\right]$, which is approximated using i) the definition $E[X] = \int_{\zeta>0}\mathbb{P}(X>\zeta)\,\mathrm{d}\zeta$, ii) the PDF in (9), and iii) Shannon's channel capacity formula, to yield

$$\begin{aligned} \mathscr{F}_a^n = \int_{\zeta>0}\Big(2\pi\lambda_b.\int_{r_t>0} r_t e^{-\pi\lambda_b r_t^2}.\; e^{-\frac{\beta_a}{P_a} r^{\alpha_a(1-\epsilon_a)}\sigma_a^2}. \\ \mathscr{L}_{I_a}\left\{\beta_a r^{\alpha_a(1-\epsilon_a)}\right\}\,\mathrm{d}r_t\Big)\,\mathrm{d}\zeta \end{aligned} \quad (12)$$

where, $\beta_a = 2^{(\zeta/\omega_a)} - 1$ and $\omega_a = (1-gb).\Omega_a/\mathscr{N}_a$ and gb is the ratio of guard band. Therefore, the mean achievable bit rate by a device is given by $\mathscr{R}_a^n = \max\{\mathfrak{L}_a^n, \mathscr{F}_a^n\}$.

Based on the above analysis and considering the first-in-first-out service rule, the total delay over the radio network, can be calculated as

$$T_{air} = \frac{T_a}{\mu_a^{n,t} - \gamma_d.\overline{\Gamma_a}} \;\; (s) \quad (13)$$

V. PLC FRONT-HAUL PERFORMANCE MODEL CALCULATION

In this section, we look at the second queue in our tandem queue model, namely, the access system delay.

A. Access system delay description

The access system delay is calculated using a Singular Value Decomposition module incorporated into the eCPG [4]. This module transforms the original 6x6 Multi Input Multi Output (MIMO) PLC channel into six parallel Single Input Single Output (SISO) channels. This simplification streamlines the analysis by focusing on SISO links. R-eCPG handles incoming eCPRI-frames, while D-eCPG manages their reception, which could be influenced by PLC channel errors and re-transmissions. In the context of eCPRI, the access system, from the RU edge to the D-eCPG edge, behaves like a G/G/1 queue. This model assumes generic incoming traffic to match the characteristics of the air interface.

In the SR process, when an eCPRI-frame enters the PLC channel, it is duplicated in R-eCPG's waiting buffer. In case of a negative acknowledgment (NACK), the eCPRI-frame is re-transmitted before new eCPRI-frames. Upon receiving an acknowledgment (ACK), the eCPRI-frame is removed from the buffer, and a new one is sent.

The access delay in this system is composed of five primary components: 1) The incoming queuing delay at R-eCPG until the new eCPRI-frame is transmitted towards the D-eCPG (T_q), 2) The transport delay through the PLC channel (T_{ts}), and 3) The processing delay related to HARQ functionality (T_{proc}).

Thus, the eCPRI-frame's access delay can be expressed as:

$$T_{PLC} = T_q + T_{ts} + T_{proc} \tag{14}$$

Therefore, the total end-to-end RAN delay is defined as

$$T_{e2e} = T_{air} + T_{PLC} \tag{15}$$

For analytical purposes, a Finite State Markov Chain (FSMC) is employed to model the behavior of eCPRI data frame transmission within each state for a single time-slot (Ts). Each eCPRI-frame Ts is set to $Ts = 66.67\ \mu s$, which corresponds to the OFDM symbol period in 5G technology. Synchronization protocols like Synchronous Ethernet (SyncE) and Precision Time Protocol (PTP) ensure temporal coherence between RU and DU in an eCPRI setup. To facilitate analysis, we assume that channel state transitions occur at the end of time slots, each representing the transmission duration of an eCPRI-frame over the PLC link. We adopt an ideal SR approximation, which separates queuing from the transmission history. Furthermore, inaccuracies in channel transitions and feedback delays are considered negligible compared to the overall state sojourn time.

The PLC channel is modeled using the Gilbert-Elliot channel model, a binary two-state finite-state Markov Chain model, for the non-stationary time-varying channel. It consists of a Good State (state 0) characterized by a low Frame Error Rate (FER) and a Bad State (state 1) characterized by high FER, with transition probabilities represented by the matrix $\mathbf{C}$. In each state, the instantaneous FER is calculated based on the probability an eCPRI-frame is received in error.

B. Radio to access network data rate conversion

The aggregated data rate received at RU_j from all scheduled devices within its coverage is calculated as $\mathscr{R}_j = \sum_{n=1}^{M_{c_j}^t} \mathscr{R}_a^n$, leading to a total incoming data rate of

$$\gamma_r = \sum_{n=1}^{M_{c_j}^t} \mu_a^{n,t} = \sum_{n=1}^{M_{c_j}^t} \left\lfloor \frac{T_a \mathscr{R}_a^n}{\mathscr{D}_a} \right\rfloor = \left\lfloor \frac{T_a \mathscr{R}_j}{\mathscr{D}_a} \right\rfloor \tag{16}$$

Let $\mathscr{D}_{p_e}$ define the size of an eCPRI-frame after the aggregation of data-frames into eCPRI frame [18]. Also, let the data rate of RU_j relayed over to the incoming buffer at its eCPG be defined as $\mathscr{R}_p^j = \Lambda_{ap}.\mathscr{R}_j$, where $\Lambda_{ap} = 2.Q_F \times \chi_e \times \nu_p$, calculated based on eCPRI split I_U (or II_D in downlink), represents the conversion factor between the data rate over the air interface and the required data rate for the eCPRI-frame to carry such data over the PLC front-haul. The quantizer resolution in the frequency domain is defined as $Q_F = 9$ and is set as the quantizer resolution for LTE [22]. The eCPRI-frame header redundancy factor and higher IP/Ethernet network layers are defined as χ_e, and ν_p is the PLC link peak utilization which is set to $\nu_p = 1$, assuming the worst case scenario [23]. The generated data rate at this stage (Split I_U) depends on the radio resource blocks utilization at the RUs (i.e., front-haul data rate is proportional to cell load).

Frequency division multiple access (FDMA) is used to split the PLC channel between the different RUs such that the bandwidth is divided into $\mathscr{N}_{plc}$ sub-channels, each of bandwidth $\omega_p = (1 - gb).\Omega_p/\mathscr{N}_{plc}$ (i.e., $\mathscr{N}_{plc}$ corresponds to the number of RUs the link can support during t^{th} TR). Therefore, the mean arrival rate of eCPRI-frames at the incoming buffer of the j^{th} R-eCPG, denoted as (γ_p^j), is defined as

$$\gamma_p^j = \left\lfloor \frac{(T_a + T_{proc}).\mathscr{R}_p^j}{\overline{\mathscr{D}_{p_e}}} \right\rfloor \tag{17}$$

where $\overline{\mathscr{D}_{p_e}}$ is the mean eCPRI-frame size. The total rate going into the PLC link for all the FDMA sub-channels is calculated as $\mathscr{R}_p = \sum_{j=1}^{\mathscr{N}_{plc}} \mathscr{R}_p^j$. This is based on the assumption that all PLC sub-channels shall be allocated. Accordingly, the total arrival rate to the SISO PLC link is defined as

$$\gamma_p = \sum_{j=1}^{\mathscr{N}_{plc}} \gamma_p^j = \left\lfloor \frac{(T_a + T_{proc}).\mathscr{R}_p}{\overline{\mathscr{D}_{p_e}}} \right\rfloor \tag{18}$$

C. Incoming Queuing Delay

The incoming queuing delay is the waiting time due to the re-transmission of other eCPRI-frames in error at the RU. Looking at the access side of the network, the

source of eCPRI-frames at the RU side is the aggregated and converted received data-frames. Therefore, the source is modeled as an N-state Discrete Markov process, where $N_{src} = 2$ is taken to represent the ON-OFF behavior of the eCPRI data flows [18], [24]. Accordingly, the transition probability matrix for the modeled source, can be calculated using the following [25], [26]

$$\rho_{pj} = \gamma_{pj}.\frac{a_{01}}{a_{01}+a_{10}} \qquad \text{and} \qquad T_{on} = \frac{1}{a_{10}} \tag{19}$$

where T_{on} is the mean length of the **ON** period, ρ_{pj} is the mean traffic load of eCPRI-frames into the j^{th} R-eCPG where $(0 < \rho_{pj} < 1/\mathcal{N}_{plc})$, $a_{01} = \mathbb{P}\{$Prob. of arrival of at least one new eCPRI-frame in current Ts with no arrival in previous $Ts\}$, $a_{10} = \mathbb{P}\{$Prob. of no arrival of new eCPRI-frame in current Ts with one new arrival in previous $Ts\}$. Moreover, $a_{00} = 1 - a_{01} = \mathbb{P}\{$Prob. of no new eCPRI-frame arrival in current Ts with no arrival in previous $Ts\}$, and $a_{11} = 1 - a_{10} = \mathbb{P}\{$Prob. of arrival of new eCPRI-frame in current Ts with one new arrival in previous $Ts\}$. The total mean traffic load into one SISO PLC link $\rho_p = \rho_{pj} \times \mathcal{N}_{plc} \ldots (0 < \rho_p < 1)$ [25].

At the k^{th} Ts, let the incoming queue length at the R-eCPG be represented as $q_z(k)$ with the channel state z, and let there be u eCPRI-frames in the queue at this Ts. Thus, the number of eCPRI-frames in the incoming queue at $Ts = (k+1)$ with channel state z and source state x at this Ts where $x, \& \ y \in \{0,1\}$ can be defined as:

$$q_{x,y}(k+1) = \begin{cases} q_{u,y}(k) + a_p(k) - r_y(k), & \text{if } q_y(k) \neq 0 \\ q_{u,1-y} + a_p(k) - r_{1-y}(k), & \text{if } q_{1-y}(k) \neq 0 \\ a_x(k), & \text{if } q_y(k) = 0, \\ & \text{or } q_{1-y}(k) = 0 \end{cases} \tag{20}$$

where $a_p(k)$ is the number of new eCPRI-frame arrivals in the k^{th} Ts. Since the assumption that one eCPRI-frame is sent per Ts is considered and that the arrival process is an ON-OFF process then $a_p(k) \in \{0, \infty\}$. The departure of an eCPRI-frame from the system is referred to as $r_y(k) \in \{0,1\}$ while the channel is in a state $y \in \{0,1\}$.

Let the current channel state (CS_k) be denoted by y and the limit of re-transmissions of an eCPRI-frame be L_r before it is dropped. The receiving of an eCPRI-frame in error or successfully depends on the current channel state and is independent of the transition in the channel state. These states will be referred to as eCPRI-frame states/ eCPRI-frame steady states. The probability of an eCPRI-frame departure from the system given either channel state is expressed as

$$r_y = \mathbb{P}\{S_0 | CS_k = y\} = \frac{1 - e_y}{1 - e_y + \alpha_p.e_y - \alpha_p.e_y^{L_r+1}} \tag{21}$$

Accordingly, the probability of no eCPRI-frame departure from the system given either channel state can be expressed as

$$v_y = \sum_{l=1}^{L_r} \mathbb{P}\{S_l | CS_k = y\} = \frac{\alpha_p.e_y.(1 - e_y^{L_r})}{1 - e_y + \alpha_p.e_y - \alpha_p.e_y^{L_r+1}} \tag{22}$$

same applies for $CS_k = 1 - y$.

With the assumptions that all launched eCPRI-frames are received at the DU, i.e. no eCPRI-frame lost over the channel, the steady state probability of the incoming queue length at the RU side $q_{x,y}[h]$ is defined as $q_{x,y}[h] \triangleq \lim_{t\to\infty} Pr\left[q_{x,y}(k) = h\right]$, which yields

$$\begin{aligned} q_{x,y}[h] = & \sum_{u=0}^{min(N_{src}, h+1)} \Big(c_{y,y} a_{u,x} r_y q_{u,y}[h-u+1] \\ & + c_{\overline{y},y} a_{u,x}.r_{\overline{y}} q_{u,\overline{y}}[h-u+1] \Big) \\ & + \sum_{u=0}^{min(N_{src}, h)} \Big(c_{y,y} a_{u,x} v_j q_{u,y}[h-u] + c_{\overline{y},y} a_{u,x} v_{\overline{y}} q_{u,\overline{y}}[h-u] \Big) \\ & + \sum_{u=0}^{min(N_{src}, 1)} \Big(c_{y,y} a_{u,x} r_y q_{u,y}[1-u] + c_{\overline{y},y} a_{u,x} r_{\overline{y}} q_{u,\overline{y}}[1-u] \Big) \\ & + c_{y,y} a_{0,x} q_{0,y}[0] + c_{\overline{y},y} a_{0,x} q_{0,\overline{y}}[0] \\ & \text{where, } \overline{y} \text{ denotes } 1-y \text{ and } x \in \{0,1\}. \end{aligned} \tag{23}$$

for the purpose of this work, $q_{0,0}[0]$ and $q_{0,1}[0]$ are initially set as zeros.

Thus, and using Little's Law, the mean queuing delay for the ideal SR HARQ scenario can be expressed as $T_q = \frac{\mathbb{E}[q]}{\rho_{pj}}$, where $\mathbb{E}[q]$ is the total mean number of eCPRI-frames at the RU side (including queuing and waiting buffers), which, considering nonzero feedback delay, is given as $\mathbb{E}[q] = \overline{q} + t_f \overline{\mathcal{T}_r} \rho_{pj}$, where $\overline{\mathcal{T}_r}$ is the mean throughput over the PLC link and $\overline{q} = \mathbb{E}[q^h_{x,y}]$ is the mean queue length in the incoming queue buffer overall source and channel states.

D. Transport Delay

The transport delay consists of 2 delays: transmission delay and propagation delay. The former is denoted as (T_t) and depends on the mean throughput ($\overline{\mathcal{T}_r}$) [24] which is expressed as $T_t = t_f.\overline{\mathcal{T}_r} - t_f/2$, where t_f is the overall feedback delay including transmission and propagation of the eCPRI-frame and of the ACK/NACK message. The propagation delay (T_{pg}) is a constant delay that depends on the length (L) of the power cable and propagation speed (v_p), where $T_{pg} = \lceil (L/v_p)/Ts \rceil$. The propagation speed (v_p) for power-lines is set to 173 $m/\mu s$ as per [27]. Based on the channel model analysis above, the mean throughput is defined as

$$\begin{aligned} & \mathcal{T}_r = 1 + \mathcal{U}\,[\mathbf{I} - \mathcal{S}]^{-1}\,\mathcal{V} \\ & \text{s.t.} \quad \mathcal{U} = \begin{bmatrix} \mathbf{1} & \mathbf{1} \end{bmatrix} \quad \mathcal{S} = \begin{bmatrix} c_{00}e_0 & c_{10}e_0 \\ c_{01}e_1 & c_{11}e_1 \end{bmatrix} \quad \mathcal{V} = \begin{bmatrix} \pi_{c_0}e_0 \\ \pi_{c_1}e_1 \end{bmatrix} \end{aligned} \tag{24}$$

where $\mathbf{I}$ is the identity matrix. π_{c_0} and π_{c_1} are the steady state probabilities that the channel is in Good and Bad states respectively; such that [28]

$$\pi_{c_0} = \frac{c_{10}}{c_{10} + c_{01}} \quad \text{and} \quad \pi_{c_1} = \frac{c_{01}}{c_{10} + c_{01}} \tag{25}$$

Consequently, the mean transport delay is calculated as $T_{ts} = T_t + T_{pg}$ [28].

VI. Numerical Results

To obtain the Gilbert-Elliot model for the PLC channel, first, the three-phase ICT OMEGA extended MIMO PLC channel with 100m in length, and the 1-300 MHz frequency bandwidth was fitted using Matlab as a Log-normal distribution with mean $\mu_p = -2.97873$ and standard deviation $\sigma_p = 1.23376$. The maximum allowable transmit power is adopted as per the power spectral density (PSD) requirements of the regulations of general Electro-Magnetic Compatibility (EMC) [29].

$$\mathbf{C} = \begin{bmatrix} 0.9466 & 0.0534 \\ 0.9090 & 0.0910 \end{bmatrix} \quad \mathbf{Fe} = \begin{bmatrix} e_0 \\ e_1 \end{bmatrix} = \begin{bmatrix} 2.8280 \times 10^{-05} \\ 0.7908 \end{bmatrix} \quad (26)$$

A matlab simulator of the RAN system analysis was set up as per the parameters in Tables II. The parameters in Table II are fixed throughout all the simulations and set as per [4], [30]. The IoT device density/ Km^2 (λ_d) is varied over the range 10K - 100K devices / Km^2 with a default value of 40K devices / Km^2. For the radio link, Narrow-band IoT (NB-IoT) 5G technology parameters were adapted. Consequently, the SINR Coverage cut-off (τ_a) is simulated using the values -20, 0, 10, 20 dB with a default value of 0 dB based on the SINR values shown in table III.

TABLE II: System simulation fixed parameters

Parameter	Value
Radio bandwidth (Ω_a)	200 KHz
Radio AWGN variance (σ_a^2)	20 dBm
Radio sub-carrier spacing (Δf_a)	15 KHz
Radio Modulation scheme	QPSK
Radio interface Scheduler	Greedy scheduler
IoT device transmit power (P_a)	23 dBm
IoT radio data frame size ($\mathscr{D}_a$) **[30]**	28 bits
Radio power control factor (ϵ_a)	0.8
Radio path-loss exponent (α_a)	4
Data packet arrival rate (γ_d)	1 data-frame/8.4s (33.3 b/s)
Radio and PLC guard band ratio (gb)	5%
Power Line Length (L_p)	100 m
MIMO PLC Ports (N_p)	6 Tx/RX ports
PLC BW / Port (Ω_p)	1 - 300 MHz
IND Threshold (Th)	10 dB
IND Mean power (P_{mean})	-115 dB
Mean eCPRI frame size ($\overline{\mathscr{D}_{pe}}$)	32770 bytes
PLC GE cut-off FER (e_{cut})	10^{-2}
Mean eCPRI on-period (T_{on})	$5Ts$
Feedback delay (t_f)	5 eCPRI-frames
HARQ Processing delay (T_{proc}) **[31]**	4 μs
HARQ retrans. Limit (L_r)	4 eCPRI-frames

TABLE III: SINR values for NB-IoT [32]

Performance Level	SINR (dB)
Excellent	≥ 20
Good	≥ 10 to <20
Fair	≥ -5 to <10
Poor	≥ -20 to <-5
Very poor	≤ - 20

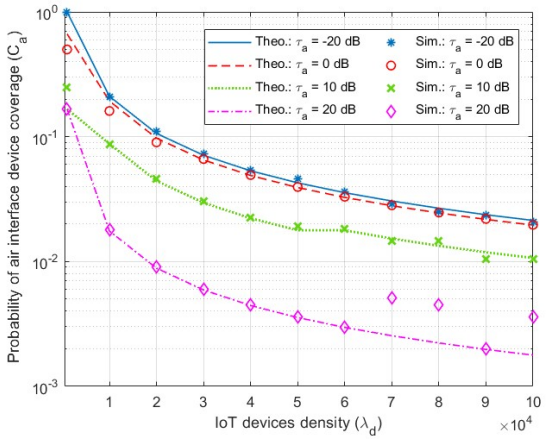

Fig. 5: Radio coverage vs. IoT devices density. λ_b = 20 RUs

Figure 5 shows the coverage probability over the air interface which, as expected, decreases as the number of devices increases. The decrease in the probability of coverage reflects the increase in interference and the radio bandwidth limitation as more devices compete for the shared resources at the RUs. At $\tau_a = -20\ dB$, and using NB-IoT parameters, a maximum of 12 devices can be scheduled at a time due to the size of the serving radio bandwidth. However, as the value for τ_a increases, the interference becomes the main limiting factor for the number of devices being served as shown in Figure 6. The effect of increasing the number of serving RUs on the coverage probability and delay performance is worth further investigation but is not included in this work.

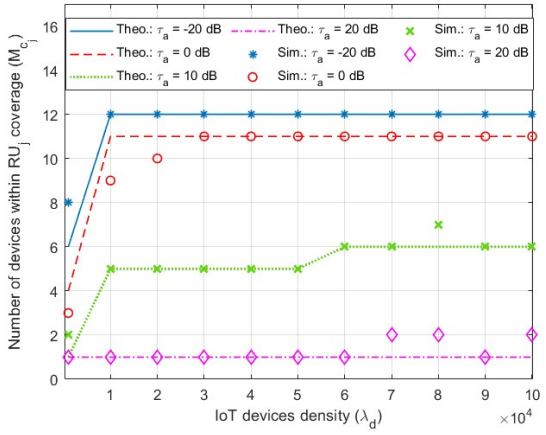

Fig. 6: Number of covered devices vs. IoT devices density. λ_b = 20 RUs

Figure 7 shows the delay over the air vs loading conditions. The delay over the radio interface is within expected limits ($< 1ms$) even when the maximum number of covered devices are being served. As the system is limited by the NB-IoT bandwidth, increasing the IoT device density doesn't have a major effect on the air interface delay. Other factors such as decreasing the number of devices per RU as well as changing the transmit power of the devices (i.e., using fractional power control methods) may have an impact on the air interface performance and may be worth further investigation.

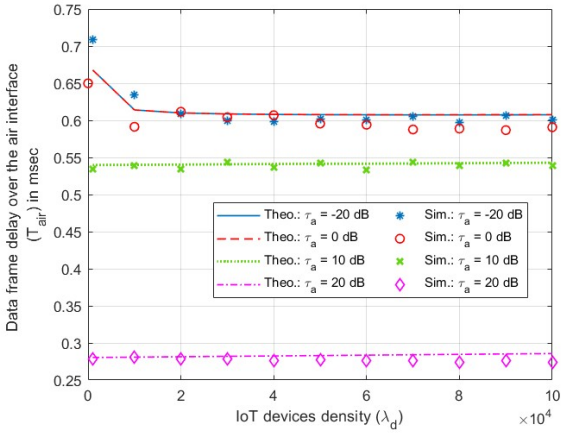

Fig. 7: Delay over air interface vs. Traffic load. λ_b = 20 RUs

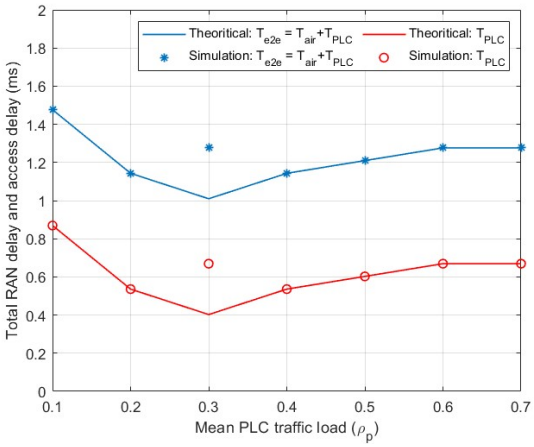

Fig. 8: Total e2e delay and access delay vs. PLC traffic load. λ_b = 20 RUs, $\tau_a = 0$ dB

In Figure 8, the end-to-end delay (air plus access) (T_{e2e}) and the access delay (T_{PLC}) are presented. As shown, with eCPRI [33] running over the PLC link, the maximum one-way delay constraint of $100ms$ is met by using any possible system parameters under low class of services as well as the delay requirement of $1ms$ for medium class of services. As for eCPRI high class of services, further research is needed to find possible ways to meet the delay requirements. Also, other factors, such as the re-sequencing delay at the receiver eCPG and the effect of the impulsive noise detection & re-transmission (IND) functionality on the delay, need to be considered to produce a comprehensive system model. However, as per the results, it is clear that the derived models accurately describe the presented system which lends confidence to our claim that PLC front-hauling could be a potential cheap alternative to support massive indoor IoT applications of the future. At $\rho_p = 0.3$, the difference between the analytical and the simulated results is equivalent to one Ts. This difference is illustrated in 9 which shows this is the difference in queue length of one eCPRI-frame due to the ceil function to the mean of the queue length generated from the system simulations of 1 million eCPRI-frames.

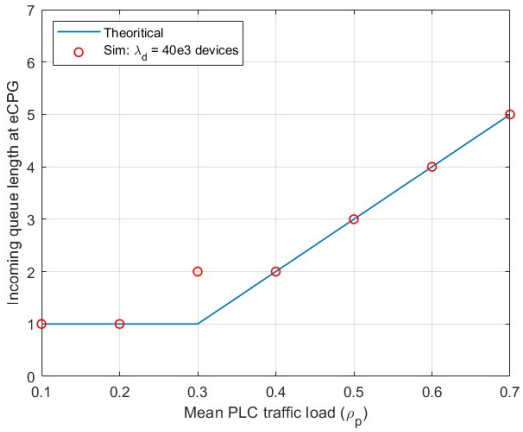

Fig. 9: eCPG incoming buffer length vs. PLC traffic load. λ_b = 20 RUs, $\tau_a = 0$ dB

VII. Conclusion

This study conducts an examination of the radio and access network delay performance within the context of a 5G indoor IoT application, where a pioneering front-haul system integrates eCPRI data frames over PLC. To analyze the intricate dynamics of such a system, the study employs a multifaceted approach, incorporating stochastic geometry, queuing theory, and finite state Markov modeling to construct analytical models for assessing network performance. The system is modeled as a tandem queue with the first queue at the IoT device and the second at the RU. Through extensive simulations that replicate real-world network topologies, the research uncovers valuable insights into critical metrics like scheduling probability, coverage probability, and radio access end-to-end delay, which are essential for understanding the system's effectiveness. It also proves the accuracy of the developed end-to-end model. Furthermore, the study tests the validity of these analytical models and the accuracy of end-to-end delay estimations, thus providing an evaluation of the proposed novel front-haul system's potential and limitations in a 5G indoor IoT scenario.

References

[1] "Technical Report on Transport network support of IMT-2020/5G, v0," Telecommunication Standardization Sector of ITU, February 2019.

[2] R. I. Rony, E. Lopez-Aguilera, and E. Garcia-Villegas, "Cost Analysis of 5G Fronthaul Networks Through Functional Splits at the PHY Layer in a Capacity and Cost Limited Scenario," *IEEE Access*, vol. 9, pp. 8733–8750, 2021.

[3] S. S. Lisi, A. Alabbasi, M. Tornatore, and C. Cavdar, "Cost-effective migration towards C-RAN with optimal fronthaul design," in *2017 IEEE International Conference on Communications (ICC)*, 2017, pp. 1–7.
[4] M. Hassan, S. H. R. Naqvi, and P.-H. Ho, "On CPRI based Fronthauling over Residential Power Lines," in *2020 International Conference on Networking and Network Applications (NaNA)*, December 2020.
[5] S. Vashi, J. Ram, J. Modi, S. Verma, and C. Prakash, "Internet of Things (IoT): A vision, architectural elements, and security issues," in *2017 International Conference on I-SMAC (IoT in Social, Mobile, Analytics and Cloud) (I-SMAC)*, 2017, pp. 492–496.
[6] C. M. R. Institute, "C-RAN The Road Towards Green RAN," White Paper,v2.5, http://labs.chinamobile.com/cran/, October 2011.
[7] C.-L. I, J. Huang, R. Duan, C. Cui, J. X. Jiang, and L. Li, "Recent Progress on C-RAN Centralization and Cloudification," *IEEE Access*, vol. 2, pp. 1030 – 1039, August 2014.
[8] C. Ranaweera, E. Wong, A. Nirmalathas, C. Jayasundara, and C. Lim, "5G C-RAN architecture: A comparison of multiple optical fronthaul networks," in *2017 International Conference on Optical Network Design and Modeling (ONDM)*, 2017, pp. 1–6.
[9] C.-L. I, C. Rowell, S. Han, Z. Xu, G. Li, and Z. Pan, "Toward Green and Soft: A 5G Perspective," *IEEE Communications Magazine*, vol. 52, no. 2, pp. 66–73, February 2014.
[10] S. Gulati, B. Natarajan, S. Kalyanasundaram, and R. Agrawal, "Performance Analysis of Centralized RAN Deployment with Non-Ideal Fronthaul in LTE-Advanced Networks," in *IEEE 83rd Vehicular Technology Conference (VTC Spring)*, May 2016.
[11] C. Cano, A. Pittolo, D. Malone, L. Lampe, A. M. Tonello, and A. G. Dabak, "State of the Art in Power Line Communications: From the Applications to the Medium," *IEEE Journal on Selected Areas in Communications*, vol. 34, no. 7, pp. 1935–1952, 2016.
[12] M. B. Hossain, M. Rahman, O. Asif, M. Rahman, and M. Chowdhury, "Broadband over Power Line (BPL): An Emerging Technology for Bangladesh," *International Journal of Communications, Network and System Sciences*, vol. 7, 09 2014.
[13] S. U. Ercan, O. Ozgonenel, and D. W. P. Thomas, "Power line communication channel for smart grid," in *2018 6th International Istanbul Smart Grids and Cities Congress and Fair (ICSG)*, 2018, pp. 208–212.
[14] A. Mathur, M. R. Bhatnagar, and B. K. Panigrahi, "Performance evaluation of PLC with log-normal channel gain over Nakagamim additive background noise," in *2015 IEEE 26th Annual International Symposium on Personal, Indoor, and Mobile Radio Communications (PIMRC)*, 2015, pp. 824–829.
[15] B. Tan and J. Tompson, "Powerline Communications Channel Modelling Methodology Based on Statistical Features," *IEEE Power Delivery Transactions*, 03 2012.
[16] L. D. Bert, P. Caldera, D. Schwingshackl, and A. M. Tonello, "On noise modeling for power line communications," in *2011 IEEE International Symposium on Power Line Communications and Its Applications*, 2011, pp. 283–288.
[17] H. Mei, M. Hassan, L. Peng, and P.-H. Ho, "A Novel Front-hauling Architecture under Centralized Radio Access Network (C-RAN)," *Journal of Communications and Networks*, vol. 24, no. 3, pp. 305–312, 2022.
[18] "Common Public Radio Interface; eCPRI Interface Specification," *eCPRI Specification V2 (2019-05-10)*, May 2019.
[19] H. G. Moussa and W. Zhuang, "RACH Performance Analysis for Large-Scale Cellular IoT Applications," *IEEE Internet of Things Journal*, vol. 6, no. 2, pp. 3364–3372, 2019.
[20] H. G. Moussa and W. Zhuang, "Energy- and Delay-Aware Two-Hop NOMA-Enabled Massive Cellular IoT Communications," *IEEE Internet of Things Journal*, vol. 7, no. 1, pp. 558–569, 2020.
[21] M. Ferraro and L. Zaninetti, "On the statistics of area size in two-dimensional thick Voronoi diagrams," *Physica A: Statistical Mechanics and its Applications*, vol. 391, p. 4575–4582, 10 2012.
[22] G. Otero Pérez, D. Larrabeiti López, and J. A. Hernández, "5G New Radio Fronthaul Network Design for eCPRI-IEEE 802.1CM and Extreme Latency Percentiles," *IEEE Access*, vol. 7, pp. 82 218–82 230, 2019.
[23] Z. Zakrzewski, "D-RoF and A-RoF Interfaces in an All-Optical Fronthaul of 5G Mobile Systems," *Applied Sciences*, vol. 10, no. 4, 2020. [Online]. Available: https://www.mdpi.com/2076-3417/10/4/1212
[24] J. G. Kim and M. M. Krunz, "Delay analysis of selective repeat ARQ for a Markovian source over a wireless channel," *IEEE Transactions on Vehicular Technology*, vol. 49, no. 5, pp. 1968–1981, 2000.
[25] F. Qasmi, M. Shehab, H. Alves, and M. Latva-Aho, "Optimum Transmission Rate in Fading Channels with Markovian Sources and QoS Constraints," in *2018 15th International Symposium on Wireless Communication Systems (ISWCS)*, 2018, pp. 1–5.
[26] S. Bjornstad, R. Veisllari, D. Chen, F. Tonini, and C. Raffaelli, "Minimizing delay and packet delay variation in switched 5G transport networks," *Journal of Optical Communications and Networking*, vol. 11, no. 4, pp. B49–B59, 2019.
[27] N. Okazima, Y. Baba, N. Nagaoka, A. Ametani, K. Temma, and T. Shimomura, "Propagation Characteristics of Power Line Communication Signals Along a Power Cable Having Semiconducting Layers," *IEEE Transactions on Electromagnetic Compatibility*, vol. 52, no. 3, pp. 756–769, 2010.
[28] H. Wen, H. Yang, C. Lin, F. Ren, Y. Yue, and J. Zhou, "Analyzing the Reliability of Group Transmission in Wireless Sensor Network," in *IEEE GLOBECOM 2008 - 2008 IEEE Global Telecommunications Conference*, 2008, pp. 1–5.
[29] M. Lanoiselée and P. Siohan, "Analog front end design for gigabit power line communication," in *2012 IEEE International Symposium on Power Line Communications and Its Applications*, 2012, pp. 170–175.
[30] A. Ijaz, L. Zhang, M. Grau, A. Mohamed, S. Vural, A. Quddus, M. Imran, C. Foh, and R. Tafazolli, "Enabling Massive IoT in 5G and beyond Systems: PHY Radio Frame Design Considerations," *IEEE Access*, vol. 4, pp. 1–1, 01 2016.
[31] D. Chitimalla, K. Kondepu, L. Valcarenghi, M. Tornatore, and B. Mukherjee, "5G fronthaul-latency and jitter studies of CPRI over ethernet," *Journal of Optical Communications and Networking*, vol. 9, no. 2, pp. 172–182, 2017.
[32] M. Sanaullah, "Coverage Measurements of Nb-IoT Technology," Master's thesis, University of Oulu, Faculty of Information Technology and Electrical Engineering, Finland, 2022.
[33] "Common Public Radio Interface: Requirements for the eCPRI Transport Network," *eCPRI Transport Network V1.2 (2018-06-25)*, June 2018.

Mai Hassan received her BS.c. and MS.c. degrees in electronics and communications engineering from the American University in Cairo in 2008 and 2013 with highest honors. She has about 10 years of experience in international companies such as Intel Labs, Huawei Technologies and Nokia Solutions and Networks. She is currently pursuing her Ph.D. studies at the University of Waterloo, Canada. Her research interests include Network control systems, Radio access networks and Mobile radio networks.

Hesham G. Moussa received his B.S. and M.S. degrees from the American University of Sharjah, Sharjah, UAE, in 2013 and 2015, respectively. He finished his Ph.D. degree at the Department of Electrical and Computer Engineering, University of Waterloo, Waterloo, ON, Canada in 2020. His current research interests include resource allocation, medium access control, quality of service provisioning in wireless networks, performance optimization for wireless machine-to-machine, and IoT communication paradigms.

Pin-Han Ho received his Ph.D. degree from Queen's University in 2002. He is currently a Professor with the Department of Electrical and Computer Engineering, University of Waterloo, Canada. He has authored/co-authored over 350 refereed technical papers and several book chapters. His current research interests cover a wide range of topics in broadband wired & wireless communication networks.